

Global Biogeochemical Cycles®



RESEARCH ARTICLE

10.1029/2023GB007880

The Influence of Air-Sea CO₂ Disequilibrium on Carbon Sequestration by the Ocean's Biological Pump

Michael Nowicki^{1,2} , Tim DeVries^{1,2} , and David A. Siegel^{1,2} 

¹Department of Geography, University of California, Santa Barbara, CA, USA, ²Earth Research Institute, University of California, Santa Barbara, CA, USA

Key Points:

- Impact of air-sea CO₂ disequilibrium on biogenic carbon inventories and sequestration times is quantified using an ocean biogeochemical model
- Air-sea CO₂ disequilibrium enhances global sequestration time by ~70 years and biogenic dissolved inorganic carbon inventory by ~35%
- Disequilibrium effect is the strongest in the Southern Ocean and North Atlantic and weakest in the Pacific Ocean

Supporting Information:

Supporting Information may be found in the online version of this article.

Correspondence to:

M. Nowicki,
mnowicki@ucsb.edu

Citation:

Nowicki, M., DeVries, T., & Siegel, D. A. (2024). The influence of air-sea CO₂ disequilibrium on carbon sequestration by the ocean's biological pump. *Global Biogeochemical Cycles*, 38, e2023GB007880. <https://doi.org/10.1029/2023GB007880>

Received 9 JUN 2023
Accepted 22 DEC 2023

Author Contributions:

Conceptualization: Tim DeVries
Data curation: Michael Nowicki
Formal analysis: Michael Nowicki
Methodology: Tim DeVries
Visualization: Michael Nowicki
Writing – original draft: Michael Nowicki, Tim DeVries
Writing – review & editing: Michael Nowicki, Tim DeVries, David A. Siegel

© 2024. The Authors.

This is an open access article under the terms of the [Creative Commons Attribution-NonCommercial-NoDerivs License](https://creativecommons.org/licenses/by/4.0/), which permits use and distribution in any medium, provided the original work is properly cited, the use is non-commercial and no modifications or adaptations are made.

Abstract The ocean's biological carbon pump (BCP) affects the Earth's climate by sequestering CO₂ away from the atmosphere for decades to millennia. One primary control on the amount of carbon sequestered by the biological pump is air-sea CO₂ disequilibrium, which is controlled by the rate of air-sea CO₂ exchange and the residence time of CO₂ in surface waters. Here, we use a data-assimilated model of the soft tissue BCP to quantify carbon sequestration inventories and time scales from remineralization in the water column to equilibration with the atmosphere. We find that air-sea CO₂ disequilibrium enhances the global biogenic carbon inventory by ~35% and its sequestration time by ~70 years compared to identical calculations made assuming instantaneous air-sea CO₂ exchange. Locally, the greatest enhancement occurs in the subpolar Southern Ocean, where air-sea disequilibrium increases sequestration times by up to 600 years and the biogenic dissolved inorganic carbon inventory by >100% in the upper ocean. Contrastingly, in deep-water formation regions of the North Atlantic and Antarctic margins, where biological production creates undersaturated surface waters which are subducted before fully equilibrating with the atmosphere, air-sea CO₂ disequilibrium decreases the depth-integrated sequestration inventory by up to ~150%. The global enhancement of carbon sequestration by air-sea disequilibrium is particularly important for carbon respired in deep waters that upwell in the Southern Ocean. These results highlight the importance of accounting for air-sea CO₂ disequilibrium when evaluating carbon sequestration by the biological pump and for assessing the efficacy of ocean-based CO₂ removal methods.

Plain Language Summary In the surface ocean, tiny organisms called phytoplankton convert CO₂ to organic matter, a portion of which is transferred to the deep ocean where it then releases CO₂. This regenerated CO₂ can be stored for hundreds to thousands of years before it is brought back to the surface ocean and reenters the atmosphere. Through this transfer of carbon from the surface to the depth, the “biological carbon pump” helps the ocean take up more CO₂ from the atmosphere. In this study, we used computer models to determine how the rate of CO₂ exchange between the ocean and the atmosphere impacts the amount of time CO₂ can be stored in the ocean. Since the air-sea exchange of CO₂ is slow, the amount of carbon stored by the biological pump is about 35% greater than it would be if the exchange happened instantly. The slow air-sea exchange rate also increases the length of time this carbon will be stored in the ocean. It is important to take this effect into account when assessing methods for deliberately storing CO₂ in the ocean.

1. Introduction

The ocean's biological carbon pump (BCP) plays an important role in determining the partitioning of carbon between the ocean and atmosphere, thereby influencing the Earth's climate. The biological pump functions as photosynthetic plankton take up dissolved inorganic carbon (DIC) in the sunlit photic zone, and the resulting particulate and dissolved organic carbon (POC and DOC, respectively) is transported to depth, or exported, as sinking particles (Boyd et al., 2019; Lampitt, Boorman, et al., 2008), by migrating animals (Archibald et al., 2019; Aumont et al., 2018), and by ocean mixing (Dall'Olmo et al., 2016; Resplandy et al., 2019). These processes help to maintain a vertical gradient in DIC in the ocean that reduces the surface ocean partial pressure of CO₂ (pCO₂), allowing the ocean to take up additional carbon from the atmosphere. The net effect of the BCP is to increase the oceanic DIC inventory by about 8% (DeVries, 2022) and reduce the atmospheric pCO₂ by approximately 200 ppm relative to what it would be without the biological pump (Parekh et al., 2006; Sarmiento & Toggweiler, 1984). Note that throughout this study, we refer only to the organic or “soft tissue” component of the biological pump and do not include the effects of the inorganic or “hard tissue” component due to the formation and dissolution of calcium carbonate (CaCO₃) exoskeletons.

The amount of DIC sequestered in the ocean due to biological activity (C_{BCP}) has been shown to depend on the carbon export rate and the sequestration time of the exported carbon once it is regenerated or “injected” (Pinti et al., 2023) as DIC in the interior ocean (Boyd et al., 2019; DeVries et al., 2012; Nowicki et al., 2022). The sequestration time refers to the amount of time that biogenic DIC will remain in the interior ocean before it is circulated back into the surface layer where it can re-enter the atmosphere. Several studies have estimated the average sequestration time of carbon exported by different biological pump pathways (Boyd et al., 2019; Nowicki et al., 2022) as well as the sequestration time for DIC released into the interior ocean (Siegel et al., 2021). These sequestration times can be convolved with rates of organic carbon respiration to determine the contribution of carbon export from different regions or mechanisms to C_{BCP} (e.g., Boyd et al., 2019; Siegel et al., 2023) or to estimate the amount of carbon that can be sequestered by purposeful injection of DIC for marine CO_2 removal (mCDR) purposes (Siegel et al., 2021).

A common issue with these previous estimates of biogenic DIC sequestration times is that they assume instantaneous equilibration of CO_2 between the atmosphere and ocean once the regenerated DIC is circulated back into the surface layer. The equilibration of CO_2 between the atmosphere and ocean is actually rather slow, with an equilibration timescale on the order of months to a year depending on factors such as the wind speed, mixed layer depth, seawater carbon buffering capacity, and ice cover (Emerson & Hedges, 2014; Sarmiento & Gruber, 2006; Williams & Follows, 2011). Simulations with ocean biogeochemical models have been used to quantify the influence of the slow air-sea CO_2 equilibration on C_{BCP} (Eggleston & Galbraith, 2018; Ito & Follows, 2013; Khatiwala et al., 2019; Marinov et al., 2008; Toggweiler et al., 2003). These studies have found that slow air-sea CO_2 equilibration increases C_{BCP} because upwelled waters that carry respired DIC to the surface in regions such as the Southern Ocean may be transported back to depth before they fully equilibrate with the atmosphere (Eggleston & Galbraith, 2018; Ito & Follows, 2013). However, the effect of air-sea CO_2 disequilibrium on the sequestration times of biogenic DIC has not yet been quantified. Additionally, previous studies have only focused on the role of air-sea disequilibrium in affecting the distribution of biogenic DIC based on where it accumulates in the interior ocean. To the best of our knowledge, no study has quantified how air-sea disequilibrium affects the inventory of injected biogenic DIC (i.e., at the location where it was regenerated via respiration) despite its relevance to biogenic carbon sequestration metrics and importance for mCDR purposes.

Here, we address these issues using simulations with a data-assimilated ocean circulation model. First, we quantify the effect of the air-sea CO_2 disequilibrium on C_{BCP} using an ocean biogeochemical model and a linearized version of this model, as described in Sections 2.1 and 2.2, respectively. Then, we demonstrate how the disequilibrium effect can be incorporated into estimates of the sequestration time of biogenic DIC, and how these estimates can be convolved with respiration rates to determine C_{BCP} , as described in Section 2.3. In Section 3, we compare these different approaches and demonstrate that they yield roughly equivalent estimates of C_{BCP} . We then use the sequestration time approach to demonstrate the effect of the air-sea CO_2 disequilibrium on global, basin-scale and regional patterns of the sequestration time of injected biogenic DIC. In Section 4, we compare our results to those of previous studies and discuss the effects of air-sea CO_2 disequilibrium on different metrics of biogenic carbon sequestration.

2. Materials and Methods

Here, we describe model simulations that we used to quantify C_{BCP} and the effect of air-sea CO_2 disequilibrium on C_{BCP} and on the sequestration time of biogenic DIC in the ocean. We first compare an ocean biogeochemical model (Section 2.1) to a linearized model (Section 2.2) in order to quantify the errors introduced by linearizing the CO_2 system chemistry. We then introduce a sequestration time model based on linearized CO_2 system chemistry in order to quantify the effects of air-sea CO_2 disequilibrium on the sequestration time of biogenic DIC (Section 2.3).

2.1. Quantifying C_{BCP} Using Ocean Biogeochemical Model Simulations

The impact of the biological pump on the oceanic DIC inventory has traditionally been estimated using ocean biogeochemical model simulations with and without biological activity (e.g., Murnane et al., 1999; Toggweiler et al., 2003). The difference between the two simulations can be attributed to the effects of the biological pump. Likewise, the models can be run with instantaneous gas exchange and realistic gas exchange rates to

quantify the impacts of incomplete air-sea CO₂ equilibration on the magnitude of the biological pump (Marinov et al., 2008).

Similar to these previous studies, we performed simulations with a steady-state data-assimilated ocean circulation inverse model (OCIM; DeVries, 2014; DeVries & Primeau, 2011), which has a horizontal resolution of 2° and 24 depth levels ranging in thickness from ~36 m near the surface to ~500 m in the deep ocean, coupled to a well-mixed atmosphere with a fixed CO₂ concentration. We ran simulations both with and without biology. For simulations with biology, the governing equation for DIC is

$$\frac{\partial \text{DIC}_{\text{tot}}(\mathbf{x})}{\partial t} = \mathbf{A} \text{DIC}_{\text{tot}}(\mathbf{x}) + \mathbf{J}_{\text{gas}}^{\text{tot}}(\mathbf{x}) + \mathbf{J}_{\text{bio}}(\mathbf{x}), \quad (1)$$

where DIC_{tot}(**x**) represents the total DIC concentration, **x** is a discrete location in the three-dimensional ocean grid, and **A** is the OCIM1 ocean circulation transport operator (DeVries, 2014). J_{bio} is the biological DIC source-sink vector (with negative values in the euphotic zone where net primary production occurs, and positive values in the aphotic zone where remineralization occurs; see global mean profile in Figure S1 of Supporting Information S1), and J_{gas}^{tot} is the transfer of CO₂ across the air-sea interface (with non-zero values only at the sea surface).

The J_{bio} values used here are taken from Nowicki et al. (2022), who implemented an ensemble of ecosystem-biogeochemical models in the OCIM1 circulation model. We use the mean J_{bio} from the ensemble of 124 data-constrained models presented in Nowicki et al. (2022). The ecosystem component of each ensemble member consists of two phytoplankton groups (small and large) and three zooplankton types (small, large non-migrating and large migrating). Each of these produces sinking POC (small or large), a fraction of which is buried in sediments at the seafloor, and releases DOC, the cycling of which is simulated with four pools of varying lability. In each ensemble member, J_{bio} fluxes were constrained to be consistent with satellite-based estimates of primary productivity and phytoplankton size distribution, as well as in situ observations of POC fluxes, DOC, dissolved oxygen and mesozooplankton. As previously mentioned, these simulations and their J_{bio} values only include the effect of the soft tissue component of the BCP, and not the carbonate component resulting from the formation and dissolution of CaCO₃ exoskeletons.

Air-sea CO₂ exchange is parameterized as being proportional to the difference between the atmospheric and seawater CO₂ partial pressure,

$$\mathbf{J}_{\text{gas}}^{\text{tot}}(\mathbf{x}) = \frac{K_w}{\Delta z_1} \alpha (p\text{CO}_{2,\text{atm}} - p\text{CO}_{2,\text{sw}}^{\text{tot}}(\mathbf{x})) \quad (2)$$

where K_w is the CO₂ gas transfer velocity, α is the solubility of CO₂ in seawater, and Δz₁ is the depth of the surface layer of the model, which is 36 m. The atmospheric CO₂ partial pressure, pCO_{2,atm}, is set to pre-industrial levels (280 μatm), while the seawater CO₂ partial pressure, pCO_{2,sw}^{tot}, is computed from the modeled total DIC concentration using CO2SYS (Lewis & Wallace, 1998). Other inputs to CO2SYS include alkalinity from the GLODAPv2 mapped climatology (Lauvset et al., 2016), and World Ocean Atlas climatology for salinity (Antonov et al., 2010), temperature (Locarnini et al., 2010), phosphate and silicate (Garcia et al., 2010).

To assess the influence of the biological pump on oceanic DIC, we ran identical simulations using Equation 1 but without the biological DIC flux (i.e., J_{bio}(**x**) = 0). This yields an estimate of the abiotic DIC (DIC_{abio}(**x**)), which is the ocean DIC concentration without the impact of biological activity. We then derive the biogenic DIC concentration, DIC_{bio}(**x**), by taking the difference between the DIC concentration in the full model with biology, and that in the abiotic model (Table 1). DIC_{bio}(**x**) represents the excess or deficit of DIC in the ocean due to the influence of biology.

To assess the influence of air-sea CO₂ disequilibrium on the biogenic DIC concentration, we ran two gas exchange scenarios with both the biotic and abiotic models. In the instantaneous gas exchange scenario, K_w was set to an arbitrarily large value (10¹⁰ m yr⁻¹) to mimic instantaneous gas exchange. In the realistic gas exchange scenario, K_w was parameterized following Ho et al. (2006) and Wanninkhof et al. (2013),

$$K_w = a(u_{10})^2(1 - f_{\text{ice}}) \left(\frac{S_c}{660} \right)^{-\frac{1}{2}}, \quad (3)$$

where a is a scale factor (22 s² m⁻¹ yr⁻¹), u₁₀ is the root-mean-square wind speed (in m yr⁻¹) at 10 m above the surface from the NCEP-DOE Reanalysis II data product, f_{ice} is the annually averaged fractional ice cover from the NCEP-DOE Reanalysis II data product, and S_c is the temperature-dependent Schmidt number for CO₂. Using

Table 1
Relevant Terms for the Different Biogenic Dissolved Inorganic Carbon Pools and Sequestration Times

	Realistic gas exchange		Instantaneous gas exchange		Disequilibrium effect	
	Method	Method	Method	Method	Method	Method
Biogenic DIC (concentration)	$DIC_{bio}(x)$	$DIC_{tot}(x) - DIC_{abio}(x)$, or Equation 4	$DIC_{bio}^{eq}(x)$	$DIC_{tot}(x) - DIC_{abio}(x)$, or Equation 4	$\Delta DIC_{bio}^{diseq}(x)$	$DIC_{bio}(x) - DIC_{bio}^{eq}(x)$
Biogenic DIC (inventory)	C_{BCP}	$\int_V DIC_{bio}(x)$	C_{BCP}^{eq}	$\int_V DIC_{bio}^{eq}(x)$	ΔC_{BCP}^{diseq}	$\int_V \Delta DIC_{bio}^{diseq}(x)$
Biogenically injected DIC (concentration)	$DIC_{bio}^{inj}(x)$	Equation 12	$DIC_{bio}^{inj,eq}(x)$	Equation 12	$\Delta DIC_{bio}^{inj,diseq}(x)$	$DIC_{bio}^{inj}(x) - DIC_{bio}^{inj,eq}(x)$
Biogenically injected DIC (inventory)	C_{BCP}^{inj}	$\int_V DIC_{bio}^{inj}(x)$	$C_{BCP}^{inj,eq}$	$\int_V DIC_{bio}^{inj,eq}(x)$	$\Delta C_{BCP}^{inj,diseq}$	$\int_V \Delta DIC_{bio}^{inj,diseq}(x)$
Mean Sequestration Time	$\mathcal{T}_S(x)$	Equation 10	$\mathcal{T}_S^{eq}(x)$	Equation 10	$\Delta \mathcal{T}_S^{diseq}(x)$	$\mathcal{T}_S(x) - \mathcal{T}_S^{eq}(x)$

these simulations, biogenic DIC can be decomposed into the sum of the biogenic DIC that would occur with instantaneous air-sea CO_2 equilibration, $DIC_{bio}^{eq}(x)$, and that due to the air-sea CO_2 disequilibrium, $\Delta DIC_{bio}^{diseq}(x)$ (Table 1). Taking the volume integral of these different DIC pools yields their total global inventory, C_{BCP}^{eq} and ΔC_{BCP}^{diseq} , respectively (Table 1).

2.2. A Linear Model for Biogenic DIC

An approximation of the effects of the biological pump on oceanic DIC concentrations can be derived using a linear model for the biogenic DIC concentration. This linearization (see Supporting Information) allows us to directly compute the biogenic DIC inventory using a single model simulation, eliminating the need to run full biotic and abiotic ocean biogeochemistry models separately to assess the differences between them. A linear formulation will also be used in our sequestration time model (Section 2.3), so the linearized biogenic DIC formulation will allow us to assess the magnitude of any errors introduced by this approximation.

Subtracting the abiotic formulation of Equation 1 from the full biotic model yields the equation for the biogenic DIC concentration,

$$\frac{\partial DIC_{bio}(x)}{\partial t} = \Delta J_{gas}^{bio}(x) + J_{bio}(x), \quad (4)$$

where $\Delta J_{gas}^{bio}(x)$ is the air-sea CO_2 flux anomaly due to the biological pump,

$$\Delta J_{gas}^{bio}(x) = -\frac{K_w}{\Delta z_1} \Delta pCO_{2,sw}^{bio}(x). \quad (5)$$

$pCO_{2,sw}^{bio}$ is the anomaly in seawater pCO_2 due to the biological pump (the difference between the seawater pCO_2 with and without biology). Note that these values are calculated for the surface layer of the model, since that is where the gas exchange occurs. The biological pCO_2 anomaly can only be fully assessed with the model simulations presented in Section 2.1, but an approximation can be derived by linearizing the CO_2 system chemistry (see Supporting Information) yielding an air-sea equilibration timescale,

$$\tau_{air-sea}(x) = \frac{\Delta z_1 \beta}{K_w R}, \quad (6)$$

where β is the equilibrium ratio of the concentration of total DIC to dissolved CO_2 in the surface ocean, and R is the Revelle buffer factor (Revelle & Suess, 1957). To compute β and R , we used CO2SYS with the same inputs used in Equation 2 but replaced the modeled DIC concentration with the modern DIC concentration from GLODAPv2 mapped climatology (Lauvset et al., 2016). Therefore, it is important to note that this air-sea equilibration timescale is specific to surface water properties derived from the modern GLODAPv2 climatology. Keeping this in mind, this timescale can be substituted into Equation 5 to yield a linear approximation for the air-sea gas exchange driven by biogenic DIC,

$$\Delta J_{\text{gas}}^{\text{bio,lin}}(\mathbf{x}) = -\frac{\text{DIC}_{\text{bio}}(\mathbf{x})}{\tau_{\text{air-sea}}(\mathbf{x})}. \quad (7)$$

Replacing $\Delta J_{\text{gas}}^{\text{bio}}(\mathbf{x})$ in Equation 4 with $\Delta J_{\text{gas}}^{\text{bio,lin}}(\mathbf{x})$ from Equation 7 yields the linearized anomaly model for biogenic DIC.

We ran this linearized anomaly model with both instantaneous and realistic gas exchange rates. In the instantaneous gas exchange scenario, $\tau_{\text{air-sea}}(\mathbf{x})$ is vanishingly small and the biological $p\text{CO}_2$ (and DIC) anomalies are therefore zero at the sea surface. In the case of realistic gas exchange, $\tau_{\text{air-sea}}(\mathbf{x})$ ranges from ~ 2 months to ~ 2 years, with the longest equilibration times in the tropics and the high-latitude ice covered regions, and the shortest equilibration time in the Southern Ocean and the subpolar North Pacific and North Atlantic (Figure S2 in Supporting Information S1). Like with the full biogeochemical model, the disequilibrium effect can be determined by taking the difference of the model with realistic gas exchange and the model with instantaneous gas exchange (Table 1).

2.3. Quantifying C_{BCP} Using the Sequestration Time of Biogenic DIC

Another method for quantifying biogenic DIC in the ocean is by tracking it from its point of injection (i.e., the location at which organic carbon is remineralized to DIC) to its removal from the ocean by air-sea gas exchange. The fate of injected biogenic DIC and its equilibration with the atmosphere can be tracked as a function of time after injection throughout the ocean using techniques previously employed to track water masses (Primeau, 2005) and the sequestration time distribution of injected CO_2 (Siegel et al., 2021), which is analogous to the “first passage time distribution” of water parcels (Primeau, 2005). This is a fundamentally different approach from those discussed in Sections 2.1 and 2.2, which solve for the accumulated concentration of biogenic DIC, or the DIC anomalies due to biological activity. The sequestration time approach instead computes the sequestration time of injected biogenic DIC, from which the time history of the inventory of biogenic DIC at its point of injection can be computed. We can then use this method to assess commonly used metrics, such as fixed depth and time horizons, for evaluating the efficiency of the biological pump (see Section 4.2).

The sequestration time distribution for biogenic DIC can be obtained by generalizing the approach used by Siegel et al. (2021), which assumed instantaneous air-sea CO_2 equilibration, to account for realistic air-sea CO_2 gas exchange. In this framework, the governing equation for the leakage rate \tilde{G} of biogenic DIC (or any tracer that exchanges with the atmosphere) from the interior ocean to the atmosphere is

$$\frac{\partial \tilde{G}(\mathbf{x}, t)}{\partial t} = \mathbf{A}^\dagger \tilde{G}(\mathbf{x}, t) - \frac{\tilde{G}(\mathbf{x}, t)}{\tau_{\text{air-sea}}(\mathbf{x})}, \quad (8)$$

where \mathbf{A}^\dagger is the adjoint of the OCIM1 transport operator, which allows us to track biogenic DIC from its point of injection in the interior ocean to its equilibration with the atmosphere. Solving Equation 8 essentially follows the temporal evolution of the boundary condition propagator \tilde{G} with the initial condition $\tilde{G} = 1 \text{ yr}^{-1}$ at the sea surface and $\tilde{G} = 0$ in the interior at $t = 0$. In the instantaneous gas exchange case, $\tau_{\text{air-sea}}(\mathbf{x}) \rightarrow 0$ which is equivalent to the boundary condition of $\tilde{G} = 0 \text{ yr}^{-1}$ at the sea surface for $t > 0$ (Siegel et al., 2021), meaning DIC is instantly removed from the ocean once it reaches the sea surface. In the realistic gas exchange scenario, once DIC reaches the surface layer, it is removed according to the air-sea equilibration timescale (i.e., $\tau_{\text{air-sea}}$) given by Equation 6. For the calculations described below, we solved Equation 8 under both instantaneous and realistic gas exchange scenarios for $t = 0$ to 7,000 years using a backward Euler time step of 1-year. This produces a distribution of times for DIC in the interior ocean to exchange with the atmosphere, since the transport operator defines pathways connecting each grid cell in the ocean to every other grid cell, yielding a nearly infinite number of possible pathways connecting an interior grid cell to a surface grid cell (e.g., Primeau, 2005).

The time dependency of \tilde{G} is made explicit in Equation 8 because this time history can be used to derive information on the distribution of sequestration times for biogenic DIC in the ocean. For instance, the fraction of biogenic DIC sequestered for t years or longer is

$$f(\mathbf{x}, t) = 1 - \int_0^t \tilde{G}(\mathbf{x}, \tau) d\tau, \quad (9)$$

Table 2

Comparison of Global Biogenic Dissolved Inorganic Carbon Inventories Computed Using Three Different Methods

	Ocean biogeochemical model	Linearized anomaly model	Sequestration time model
C_{BCP} (Pg C)	1,780	1,751	1,751
C_{BCP}^{eq} (Pg C)	1,293	1,293	1,293
ΔC_{BCP}^{diseq} (Pg C)	487	458	458

and integrating this function over all possible sequestration times yields the mean sequestration time, or the amount of time on average before DIC injected at location \mathbf{x} will exchange with the atmosphere,

$$\mathcal{T}_S(\mathbf{x}) = \int_0^{\infty} f(\mathbf{x}, \tau) d\tau. \quad (10)$$

We perform these calculations for both the realistic and instantaneous gas exchange cases to obtain the mean sequestration times for each case ($\mathcal{T}_S^{eq}(\mathbf{x})$ and $\mathcal{T}_S^{diseq}(\mathbf{x})$, respectively, in Table 1).

The sequestration time model can be used to quantify the oceanic inventory of biogenic DIC just as the ocean biogeochemical model simulations do.

However, in the sequestration time model DIC_{bio} is quantified at the point of injection (i.e., when organic carbon is converted to DIC), whereas in the biogeochemical model DIC_{bio} is quantified at the point of accumulation due to ocean circulation after it has been injected. Furthermore, in the sequestration time model DIC_{bio} can also be quantified by the time since injection, whereas in the biogeochemical model this tracking is not possible. For example, the amount of biogenic carbon that is injected at location \mathbf{x} and that is sequestered for t years or less in the ocean is given by

$$DIC_{bio}^{inj}(\mathbf{x}, t) = \int_0^t J_{bio}(\mathbf{x}, t - \tau) f(\mathbf{x}, \tau) d\tau, \quad (11)$$

where for our calculations J_{bio} is the same steady-state climatological biological source-sink term used in the ocean biogeochemical model simulations (Section 2.1). The “inj” superscript refers to biogenic DIC at the injection point to distinguish this DIC_{bio} from those in Section 2.1 (i.e., DIC_{bio} accumulated due to circulation). Assuming that J_{bio} is a constant, combining Equations 9–11 and using $t = \infty$ yields an expression for the biogenic DIC inventory at steady-state,

$$DIC_{bio}^{inj}(\mathbf{x}) = J_{bio}(\mathbf{x}) \mathcal{T}_S(\mathbf{x}). \quad (12)$$

Like for the ocean biogeochemical model simulations, these calculations can be done with both instantaneous and realistic gas exchange rates (by varying $\tau_{air-sea}$ appropriately in Equation 8), and the total biogenic DIC concentration can be expressed as the sum of the concentration that would exist if there were instantaneous air-sea CO_2 equilibration, $DIC_{bio}^{eq, inj}(\mathbf{x})$, and the difference in concentrations due to air-sea disequilibrium, $\Delta DIC_{bio}^{diseq, inj}(\mathbf{x})$ (Table 1).

3. Results

3.1. Global Biogenic DIC Inventory and the Effect of Air-Sea Disequilibrium

Each of methods described above (Sections 2.1–2.3) produces an estimate of the global biogenic DIC inventory (C_{BCP}) under both instantaneous and realistic gas exchange assumptions, which can be used to compute C_{BCP}^{eq} and ΔC_{BCP}^{diseq} , as shown in Table 2. The total amount of carbon sequestered by the biological pump is the sum of C_{BCP}^{eq} and ΔC_{BCP}^{diseq} , which ranges from 1,751 Pg C in the linearized models to 1,780 Pg C in the ocean biogeochemical model.

In the instantaneous gas exchange scenario, the global inventory (C_{BCP}^{eq}) estimated by each method is identical at 1,293 Pg C. This equivalence is expected because in the limit of instantaneous gas exchange, the linearized equations are identical to the full non-linear carbon cycle equations since the seawater and atmospheric pCO_2 are identical in both the abiotic and biotic models, and thus $pCO_{2,sw}^{bio} = 0$ (Equation 4). The biological carbon sequestration estimates of Nowicki et al. (2022) were based on this instantaneous gas exchange limit. The magnitude of ΔC_{BCP}^{diseq} in the full ocean biogeochemical model is 487 Pg C, while in the linearized anomaly and sequestration time models the magnitude is slightly lower at 458 Pg C. This shows that our linearization of the CO_2 system chemistry underestimates ΔC_{BCP}^{diseq} by about 6% (see Section 4.3 for further discussion).

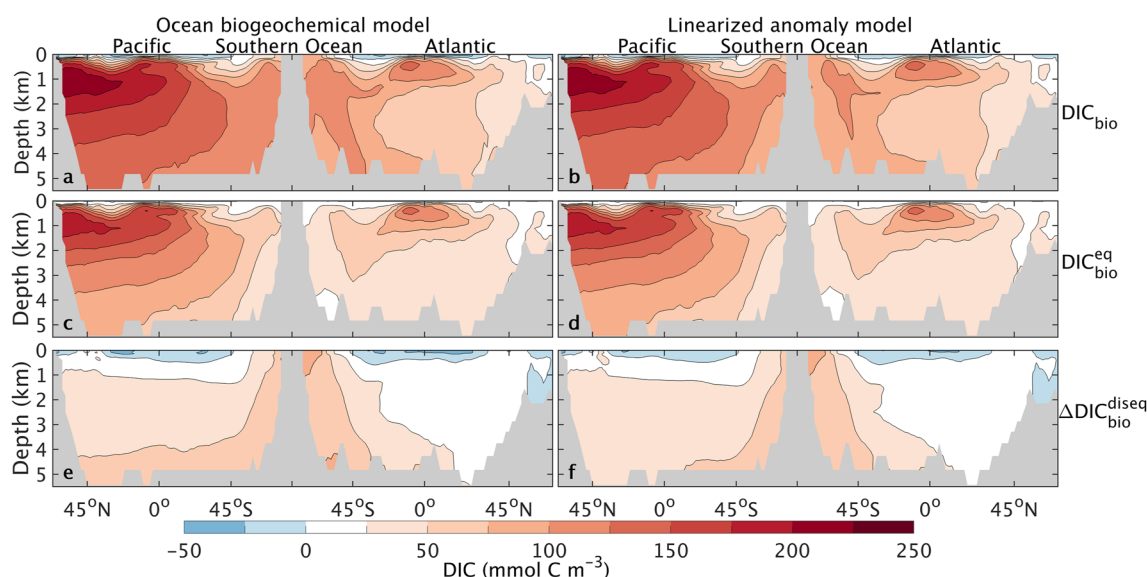


Figure 1. Comparison of zonally averaged biogenic dissolved inorganic carbon computed from the full biogeochemical models (see Section 2.1; Equation 1) (left column) and the linearized anomaly model (see Section 2.2; Equation 4) (right column). Both the (a and b) realistic and (c and d) instantaneous gas exchange scenarios are shown, as well as the disequilibrium effect (realistic gas exchange—instant gas exchange; e, f).

The spatial distribution of DIC_{bio} , and of the equilibrium ($\text{DIC}_{\text{bio}}^{\text{eq}}$) and disequilibrium components ($\Delta\text{DIC}_{\text{bio}}^{\text{diseq}}$), is shown in Figure 1 for both the full biogeochemical model and the linearized anomaly model. The spatial distribution of $\text{DIC}_{\text{bio}}^{\text{eq}}$ estimated by these two models are identical (Figures 1c and 1d). Their spatial distributions in the realistic gas exchange scenario are not quite identical, but as with their estimates of C_{BCP} (Table 2), the discrepancies are small. The disequilibrium effect ($\Delta\text{DIC}_{\text{bio}}^{\text{diseq}}$) in the biogeochemical model (Figure 1e) is slightly larger than that in the linearized anomaly model, particularly in the Southern Ocean and bottom waters ventilated from the Southern Ocean (Figure 1f). In the biogeochemical model, the zonally averaged $\Delta\text{DIC}_{\text{bio}}^{\text{diseq}}$ is $\sim 7\%$ larger than in the linearized anomaly model in the deep North Pacific and Southern Ocean below $\sim 1,500$ m. In the low-latitude surface ocean where $\Delta\text{DIC}_{\text{bio}}^{\text{diseq}}$ is negative, values are $\sim 7\%$ greater in the linearized anomaly model than in the nonlinear biogeochemical model (Figures 1e and 1f).

$\text{DIC}_{\text{bio}}^{\text{eq}}$ and $\Delta\text{DIC}_{\text{bio}}^{\text{diseq}}$ have different spatial patterns and magnitudes (Figure 1). The North Pacific is the largest reservoir for $\text{DIC}_{\text{bio}}^{\text{eq}}$ with a zonally averaged $\text{DIC}_{\text{bio}}^{\text{eq}}$ maximum of $200 \text{ mmol C m}^{-3}$ at $\sim 1,000$ m (Figures 1c and 1d). This corresponds with the nutrient maximum in the poorly ventilated North Pacific “shadow zone” (Holzer et al., 2021). $\Delta\text{DIC}_{\text{bio}}^{\text{diseq}}$ is greatest in the Southern Ocean, reaching values of up to 75 mmol C m^{-3} in the Atlantic sector near the surface (Figures 1e and 1f). In majority of the ocean, the net effect of the biological pump is to increase the inventory of accumulated DIC, but in the tropical and subtropical surface waters, the biological pump actually reduces DIC accumulation (Figures 1a and 1b; blue contours). This effect is due to air-sea CO_2 disequilibrium (Figures 1e and 1f). In the tropical and subtropical surface ocean, primary production reduces the DIC concentration, and air-sea gas exchange is unable to completely compensate for this effect by taking up more CO_2 from the atmosphere because of the slow air-sea CO_2 equilibration. Contrastingly, in the Southern Ocean the upwelling of biogenic DIC from subsurface waters creates an excess of DIC that is prevented from fully outgassing to the atmosphere by air-sea CO_2 disequilibrium, leading to a positive $\Delta\text{DIC}_{\text{bio}}^{\text{diseq}}$ in surface waters here. This supports previous findings that air-sea CO_2 disequilibrium in the Southern Ocean is the primary driver of the net positive effect of air-sea disequilibrium on C_{BCP} (Eggleston & Galbraith, 2018; Ito & Follows, 2013).

3.2. Sequestration Time of Biogenic DIC and the Effect of Air-Sea Disequilibrium

Having established that the linearized anomaly model accurately captures the effects of air-sea disequilibrium in the full ocean biogeochemical model, we can use the linearized sequestration time model (Section 2.3) to quantify the effects of the air-sea CO_2 disequilibrium on biogenic carbon sequestration times. The average sequestration time of biogenic DIC with realistic gas exchange (\mathcal{T}_s) ranges from less than 100 years near the sea

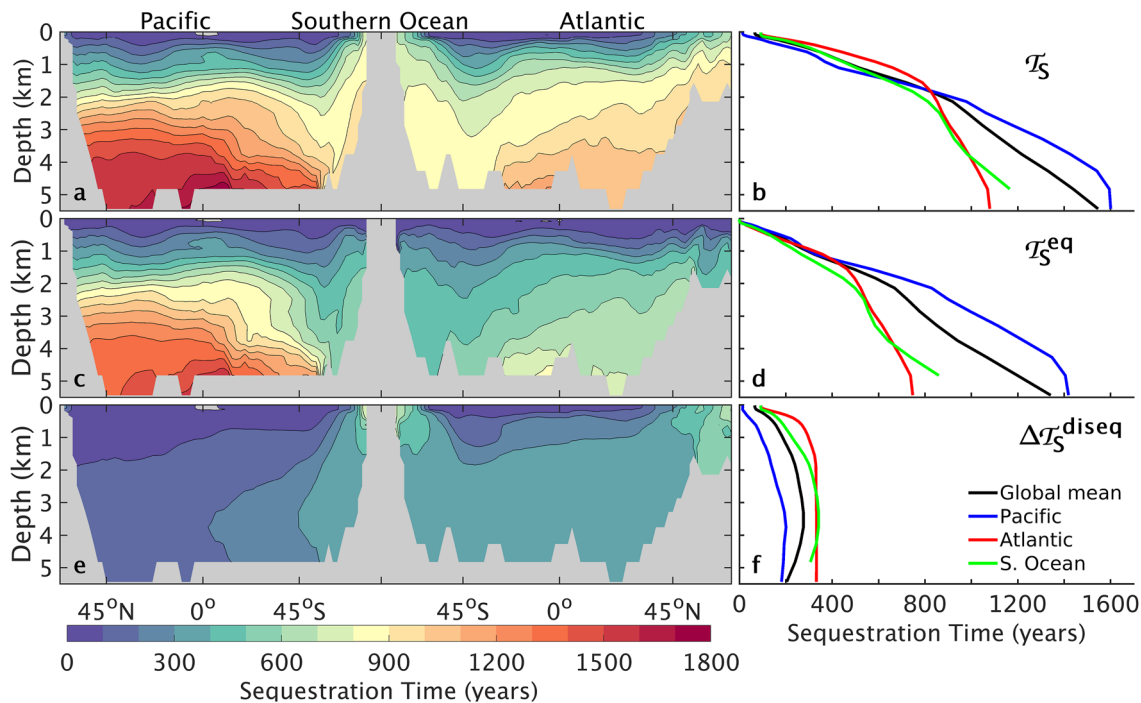


Figure 2. Zonally averaged sequestration time for the Pacific, Atlantic, and Southern Oceans under realistic (a) and instantaneous (c) gas exchange scenarios. Panel (e) shows the impact of the air-sea CO_2 disequilibrium on the sequestration time (realistic gas exchange—instantaneous gas exchange). Panels (b, d, and f) show the corresponding depth profiles for the global- and basin-averaged sequestration times. The Pacific and Atlantic basins refer to waters north of $\sim 45^\circ\text{S}$ in these basins. The Southern Ocean refers to waters south of $\sim 45^\circ\text{S}$.

surface to roughly 1,600 years in the deep North Pacific (Figures 2a and 2b). In the deep ocean, carbon sequestration times are much longer in the Pacific than in the Atlantic Ocean, reflecting the fact that the Atlantic Ocean is more rapidly ventilated by the ocean's overturning circulation. With instantaneous air-sea CO_2 equilibration, the mean sequestration times ($\mathcal{T}_S^{\text{eq}}$) are everywhere shorter than with realistic gas exchange, but the inter-basin differences remain similar (Figures 2c and 2d). $\mathcal{T}_S^{\text{eq}}$ is identical to the mean sequestration times presented by Siegel et al. (2021), which were calculated assuming instantaneous air-sea equilibration.

The difference between the sequestration time with realistic and instantaneous gas exchange is considered the disequilibrium sequestration time ($\Delta\mathcal{T}_S^{\text{diseq}}$) (Table 1; Figures 2e and 2f). Globally, air-sea CO_2 disequilibrium increases the average sequestration time of biogenic DIC by ~ 75 years for DIC injected near the surface and ~ 200 years for DIC injected in the deep ocean, with a peak of slightly over 300 years at $\sim 3,500$ m (Figure 2f). Locally, the largest disequilibrium effect occurs in the Southern Ocean and North Atlantic above $\sim 1,000$ m, where air-sea disequilibrium increases the zonally averaged sequestration time of biogenic DIC injected in these regions by more than 600 years (Figure 2e). This reflects the inefficiency of air-sea CO_2 equilibration in these regions of deep-water formation. In the Southern Ocean, rapid circulation due to upwelling along the Polar Front, combined with subduction north of the Polar Front and deep-water formation along the Antarctic margin (Ito & Follows, 2013; Toggweiler & Samuels, 1995) gives biogenic DIC in the surface waters little time to equilibrate with the atmosphere, so subducted water parcels are not in equilibrium with the atmosphere. Sea ice coverage can also play a role in preventing surface waters from contacting the atmosphere and subsequently outgassing biogenic DIC (Ferreira et al., 2018), effectively increasing the sequestration time. Similarly, air-sea CO_2 disequilibrium enhances sequestration times in the North Atlantic due to deep water formation, which results in incomplete equilibration of surface waters before they are subducted (Follows & Williams, 2004).

The disequilibrium effect is weakest in the Pacific Ocean, where $\Delta\mathcal{T}_S^{\text{diseq}}$ is negligible near the surface and ~ 150 years in the deep ocean. Surface waters of the Pacific Ocean are better equilibrated than those in the Southern or Atlantic Oceans, which is due to differences in the circulation dynamics of these basins (keep in mind the values shown in Figure 2 are basin-averaged). In the Pacific Ocean, upwelling of DIC_{bio} -rich waters occurs primarily in the Eastern Equatorial Pacific and Northwest Pacific (Sarmiento & Gruber, 2006). These

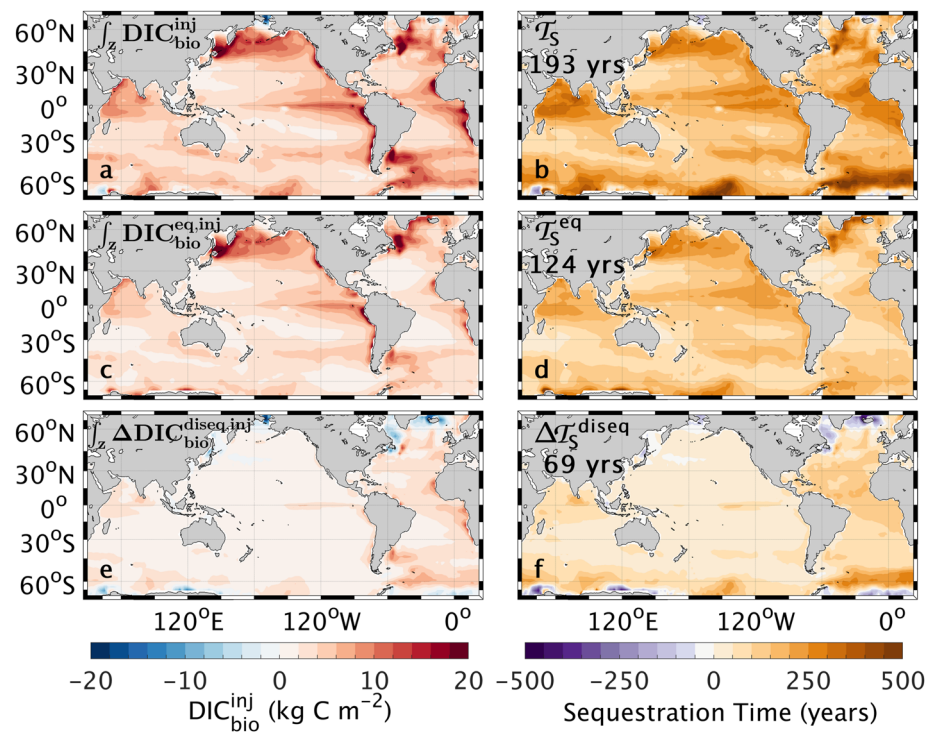


Figure 3. Left-hand column shows the vertical integral of the total injected biogenic dissolved inorganic carbon with realistic gas exchange (a; see Equation 12), with instantaneous gas exchange (c; see Equation 12), and the effect due to air-sea CO₂ disequilibrium (e; a minus c). Right-hand column (b, d, and f) shows the average sequestration time of exported carbon under each scenario, calculated by dividing the total vertically integrated carbon sequestration (left-hand column) by the carbon export at each location (approximated as the vertical integral of remineralization within each water column). Values printed on panels (b, d, and f) are globally averaged sequestration times for each gas exchange scenario.

regions are not associated with deep-water formation regions, and thus excess biogenic DIC in upwelled waters is able to equilibrate with the atmosphere. The intermediate waters of the Pacific exhibit stagnant circulation compared to the Southern and Atlantic Oceans (de Lavergne et al., 2017; Holzer et al., 2021), and these waters are partially ventilated by mode and intermediate waters that are better equilibrated than waters formed in the polar regions. The deep Pacific is primarily ventilated by Antarctic Bottom Waters (Holzer et al., 2021), which have a larger air-sea disequilibrium that causes them to have longer disequilibrium sequestration times than intermediate waters (Figure 2f).

3.3. Air-Sea CO₂ Disequilibrium Effect on Biogenic DIC Sequestration

The mean sequestration times illustrated in Section 3.2 can be convolved with the biological DIC flux (J_{bio}) to yield the total carbon sequestered by the biological pump (Equation 12). We note again that this calculation quantifies the biogenic DIC inventory at the location where the DIC is remineralized (i.e., the injection location) and, as such, is closely tied to the location of carbon export. Vertically integrating this 3-dimensional field yields the carbon sequestration due to the biogenic DIC fluxes throughout the water column, which can be viewed as a map of the contribution of the biological pump to carbon sequestration (Figure 3a). This map reveals that carbon sequestration by the biological pump is largest in the North Atlantic, North Pacific, and the eastern boundary upwelling regions in the Pacific and Atlantic Oceans (Figure 3a). These regions all have water column carbon sequestration inventories of greater than 10 kg C m⁻². Furthermore, the mean sequestration time of biogenic DIC can be determined for each location by dividing the total carbon sequestration by the vertically integrated carbon remineralization rate. Since most carbon remineralization occurs in the same vertical water column where it is exported in our model, the vertically integrated carbon remineralization rate is very close to the carbon export at each location. This calculation reveals that the sequestration time of exported carbon averages 193 years, with significant spatial variability (Figure 3b). Sequestration times are longest in the Southern Ocean, where mean sequestration times exceed 500 years near the Antarctic margin. Sequestration times are also high (>250 years) in

the North Atlantic and North Pacific as well as the equatorial upwelling and eastern boundary upwelling regions, while sequestration times are lowest in the subtropical gyres and western boundary current regions (Figure 3b).

The carbon sequestration that would occur with instantaneous air-sea CO₂ equilibration and the corresponding sequestration time of exported carbon are shown in Figures 3c and 3d. This has been discussed before (cf., Nowicki et al. (2022), their Figure 6), but here we will note that the mean biogenic DIC sequestration time of 124 years with instantaneous air-sea CO₂ equilibration is significantly shorter than the 193 years with realistic gas exchange. The difference is attributed to air-sea CO₂ disequilibrium (Figures 3e and 3f). In most regions of the ocean, the disequilibrium effect enhances the ability of the biological pump to store carbon in the ocean (Figure 3e) and increases the sequestration time of exported carbon (Figure 3f; global average of 69 years). Air-sea CO₂ disequilibrium enhances carbon sequestration inventories and sequestration times the most for carbon exported in the Atlantic Ocean and the Southern Ocean (recall that these quantities are all tied to the location where the DIC is first injected, not where it resurfaces). In these regions, air-sea disequilibrium enhances the sequestration time of injected biogenic DIC by 50–200 years. Presumably this is because biogenic DIC injected in these regions preferentially resurfaces in the Southern Ocean (DeVries & Primeau, 2011), a region where large air-sea CO₂ disequilibrium prevents the outgassing of biogenic DIC (Ito & Follows, 2013; Takahashi et al., 2009). Air-sea CO₂ disequilibrium enhances the strength of the biological pump in the Indian Ocean as well, although the effect is smaller than in the Atlantic and Southern Oceans, while in the Pacific Ocean the disequilibrium effect is very small (Figures 3e and 3f).

Interestingly, there are some regions where the disequilibrium effect weakens the ability of the biological pump to sequester carbon. This is seen most prominently in the Southern Ocean along the Antarctic margin, and the subarctic North Atlantic in the Labrador Sea and Nordic Seas (Figure 3e), which are all regions of deep-water formation. In these regions, biological uptake reduces the CO₂ concentration in surface waters to below saturation, and these waters are then subducted before they can take up additional CO₂ from the atmosphere. Thus, while the global effect of the air-sea CO₂ disequilibrium is to enhance the biogenic DIC inventory by preventing the outgassing of upwelled respired DIC, locally, air-sea CO₂ disequilibrium can reduce the efficiency of the biological pump. In deep-water formation regions, we find that air-sea disequilibrium can reduce the sequestration time of biogenic DIC by about 50–100 years (Figure 3f).

4. Discussion

We now shift our focus to discussing our results as they relate to previous studies on carbon sequestration by the biological pump. We then look at sequestration metrics that are commonly used to evaluate the biological pump and to quantify the potential of some marine CO₂ removal (mCDR) methods, and we evaluate the impact of air-sea CO₂ disequilibrium on these metrics. Lastly, we discuss important caveats to consider when interpreting our results.

4.1. Comparison to Previous Studies

Here, we compare our estimates of C_{BCP}^{eq} and C_{BCP}^{diseq} to estimates from a variety of previous studies (Table 3). Numerous studies have estimated C_{BCP}^{eq} , where it has also been called DIC_{soft} (e.g., Eggleston & Galbraith, 2018), C_{org} (Ito & Follows, 2005), or C_{bio} (Ito & Follows, 2013) (Table 3). Eggleston and Galbraith (2018) used an Earth system model (ESM) under various preindustrial and last glacial maximum configurations and calculated a C_{BCP}^{eq} ranging from 900 to 1,800 Pg C. Khatiwala et al. (2019) found a C_{BCP}^{eq} of 971 Pg C using an ESM configured for preindustrial conditions. Marinov et al. (2008) found that C_{BCP}^{eq} ranged from 1,278 to 2,350 Pg C in a suite of biogeochemical models configured under different idealized conditions. For the modern ocean, Wilson et al. (2022) computed values ranging from ~1,625 to 2,150 Pg C for C_{BCP}^{eq} based on the apparent oxygen utilization (AOU) from an ensemble of seven CMIP6 models. However, the AOU approach may overestimate C_{BCP}^{eq} due to oxygen undersaturation in deep water formation regions, leading to an overestimate of respiration (Ito et al., 2004).

Observation-based estimates of preformed nutrients and oxygen in the ocean have also been used to calculate C_{BCP}^{eq} . Ito and Follows (2005) used AOU observations to estimate that about 36% of the phosphate in the ocean is derived from regenerated organic matter. At a C:P ratio of 106:1 (Redfield, 1934) and a mean ocean phosphate concentration of 2.2 μmol/kg, this implies a C_{BCP}^{eq} of about 1,340 Pg C. Similarly, Carter et al. (2021)

Table 3
Comparison With Previous Studies

	C_{BCP}^{eq} (Pg C)	ΔC_{BCP}^{diseq} (Pg C)	Method
This study	1,293	487/458 (+35%)	Ocean biogeochemical model/linearized model
Eggleston and Galbraith (2018)	900–1,800 ^a	NR ^b	Earth system model ensemble
Khawiwala et al. (2019)	971 ^c	1,079 ^d (+111%)	Earth system model
Marinov et al. (2008)	1,278–2,350 ^e	NR ^b	Ocean biogeochemical model ensemble
Wilson et al. (2022)	~1,625–2,150 ^c	NR ^b	Ensemble of CMIP6 models using AOU
Ito and Follows (2005)	1,340 ^f	NR	AOU and nutrient observations
Carter et al. (2021)	1,300 ± 230	NR ^b	Data-based preformed nutrients/oxygen
Toggweiler et al. (2003)	NR ^b	+33%/+60%	3-box model/ocean biogeochemical model
Ito and Follows (2013)	NR ^b	+70%	Idealized GCM

^aReferred to as DIC_{soft}. ^bValue not reported. ^cReferred to as C_{soft}. ^dReferred to as C_{dis, bio}. ^eReferred to as OCS_{soft}. ^fReferred to as C_{org}.

used data-based estimates of preformed nutrients and oxygen to estimate a C_{BCP}^{eq} of 1,300 (± 230) Pg C. These data-based estimates match up well with our model estimate for C_{BCP}^{eq} of 1,293 Pg C, which is consistent with the fact that our model is constrained by ocean oxygen observations.

Compared to C_{BCP}^{eq} , fewer estimates of C_{BCP}^{diseq} can be found in the literature (Table 3). Our data-constrained model suggests that air-sea CO₂ disequilibrium increases the carbon stored by the biological pump by 487 Pg C, which is a 35% increase compared to the carbon stored by the biological pump under instantaneous gas exchange. This is similar to the 33% increase in biological pump strength found by Toggweiler et al. (2003) using the difference in the surface to deep DIC in an “organic only” version of a simple box model run with standard and fast gas exchange. Toggweiler et al. (2003) also ran “organic only” versions of an ocean biogeochemistry model with standard and fast gas exchange, finding a 60% increase in the strength of the biological pump due to air-sea CO₂ disequilibrium. Other recent studies have found even larger effects. Ito and Follows (2013) performed a suite of experiments with an ocean biogeochemical model and estimated a 70% increase in biogenic carbon inventory due to air-sea CO₂ disequilibrium, and Khawiwala et al. (2019) diagnosed a C_{BCP}^{diseq} of 1,079 Pg C using an ESM configured in a preindustrial state (Table 3).

Most of the previous estimates of C_{BCP}^{diseq} from ocean biogeochemical models show a much larger impact of air-sea disequilibrium on the biological pump (60%–111% increase) compared to our results (35% increase). It is not fully clear what causes this difference, but it is unlikely to be caused by differences in the air-sea CO₂ gas transfer velocity because all models use similar parameterizations for this process. It is more likely related to differences in ocean circulation and/or carbon export among the models. We hypothesize that it could be related to the magnitude of carbon export in the Southern Ocean in particular. Our results demonstrate that the Southern Ocean is the crucial region where air-sea CO₂ disequilibrium can increase the sequestration time of exported carbon, particularly the region near 60°S (Figure 3f). In fact, in this region of the Southern Ocean, the disequilibrium sequestration time meets or exceeds the equilibrium sequestration time (Figures 3d and 3f). Thus, the magnitude of C_{BCP}^{diseq} is closely tied to how much carbon export occurs in this region. Our model uses satellite-based estimates of NPP, which may be too low in the Southern Ocean south of 50°S (Schlitzer, 2002). In particular, satellite NPP products lack data poleward of 65°S, which causes very low carbon export in this region (Nowicki et al., 2022). This could bias our estimates of C_{BCP}^{diseq} too low. Another potential source of bias in our estimates of C_{BCP}^{diseq} is the OCIM’s lack of seasonally varying circulation. The extent to which unresolved seasonality in the OCIM may bias our estimates of C_{BCP}^{diseq} is unclear, but any such effect would likely be seen most prominently in regions like the Southern Ocean, which exhibits large seasonality in processes important to C_{BCP}^{diseq} such as sea ice extent and deep-water formation (Morley et al., 2020; see Section 4.3 for further discussion of caveats). However, it is also possible that C_{BCP}^{diseq} is misrepresented in coarse-resolution GCMs, since these models have serious deficiencies in their representation of deep convection in the Southern Ocean (Heuzé et al., 2013; Li et al., 2023), which could bias their estimates of carbon export and air-sea disequilibrium in this region. Relative to free-running coarse-resolution GCMs, the circulation of the OCIM is improved by the assimilation of tracer data such as radiocarbons and CFCs (DeVries, 2014).

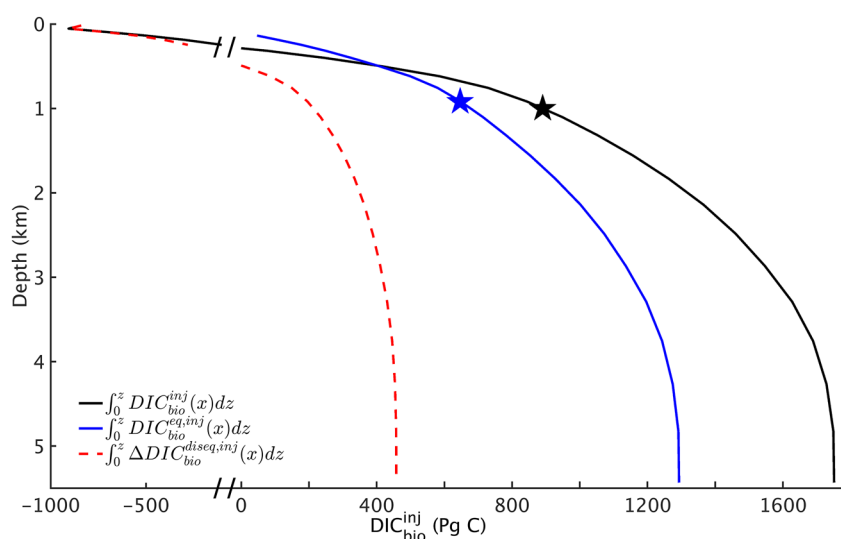


Figure 4. Globally integrated biogenic dissolved inorganic carbon (DIC) due to injection above each depth level in Pg C. Both the instantaneous (blue line) and realistic (black line) gas exchange scenarios are shown, as well as the disequilibrium effect (realistic gas exchange—instant gas exchange; dashed red line). Stars indicate the depth above which 50% of the DIC inventory is sequestered due to injection. Note the break in the x-axis at 0 Pg C. Calculations are performed by integrating Equation 12 from the sea surface to the depth on the y-axis, as indicated in the legend.

4.2. Impact of Air-Sea Disequilibrium on Sequestration Metrics for the Biological Pump

A commonly used metric for assessing the sequestration efficiency of the biological pump is the flux of organic carbon reaching the deep ocean. This is generally set at a fixed depth horizon, typically 1,000 m (Passow & Carlson, 2012; Robinson et al., 2014) or 2,000 m (Guidi et al., 2015). The flux passing this depth horizon is commonly considered to be the only flux that can contribute to long-term carbon sequestration and therefore be climatically relevant (Baker et al., 2022). However, sequestration time calculations assuming instantaneous air-sea CO_2 equilibration have revealed that in fact roughly half of the biogenic DIC inventory in the ocean is due to the respiration of organic carbon above 1,000 m (Siegel et al., 2023). This is shown in Figure 4, which illustrates the carbon sequestration due to respiration above a given depth horizon for the instantaneous and realistic gas exchange scenarios. With instantaneous gas exchange, $\sim 1,300$ Pg C is sequestered due to injection above the seafloor (i.e., the entire $DIC_{bio}^{eq,inj}$) and half of this is due to respiration that occurs above ~ 900 m (blue star in Figure 4).

With our disequilibrium sequestration time calculations, we can also assess the impact of air-sea CO_2 disequilibrium on the depth distribution of biogenic carbon sequestration. Unlike $DIC_{bio}^{eq,inj}$, which is positive everywhere, $\Delta DIC_{bio}^{diseq,inj}$ only becomes positive below about 500 m (Figure 4). Above this depth, the integrated effect of the air-sea CO_2 disequilibrium is to weaken the biological pump, due to biological DIC uptake in the euphotic zone. In a mathematical sense (see Equation 12), this can be understood by considering that the disequilibrium sequestration time ($\Delta \mathcal{T}_S^{diseq}$) is positive at the sea surface (Figures 2e and 2f), while J_{bio} is negative in the euphotic zone due to biological DIC uptake (i.e., NPP; see Figure S1 in Supporting Information S1). This leads the disequilibrium carbon sequestration ($\Delta DIC_{bio}^{diseq,inj}$) to be negative in the euphotic zone. Conceptually, this can be understood because biological DIC uptake in the euphotic zone causes CO_2 deficits relative to saturation. Since air-sea CO_2 disequilibrium prevents the uptake of CO_2 from the atmosphere, the disequilibrium effect in response to biological DIC uptake reduces the biogenic DIC inventory relative to the instantaneous gas exchange scenario. It is only when the organic carbon is regenerated in the subsurface, and the resulting excess DIC is upwelled to the surface that the air-sea CO_2 disequilibrium effect becomes positive by preventing the outgassing of this excess CO_2 to the atmosphere. This means if the total amount of biological DIC uptake remained the same, but DIC regeneration were limited to the amount that occurs above 500 m, the air-sea CO_2 disequilibrium would have a net zero effect on the strength of the biological pump. Considering the fully depth-integrated inventory, however, the air-sea CO_2 disequilibrium effect increases the net storage of DIC by the biological pump by about 450 Pg C (red curve in Figure 4 at the seafloor).

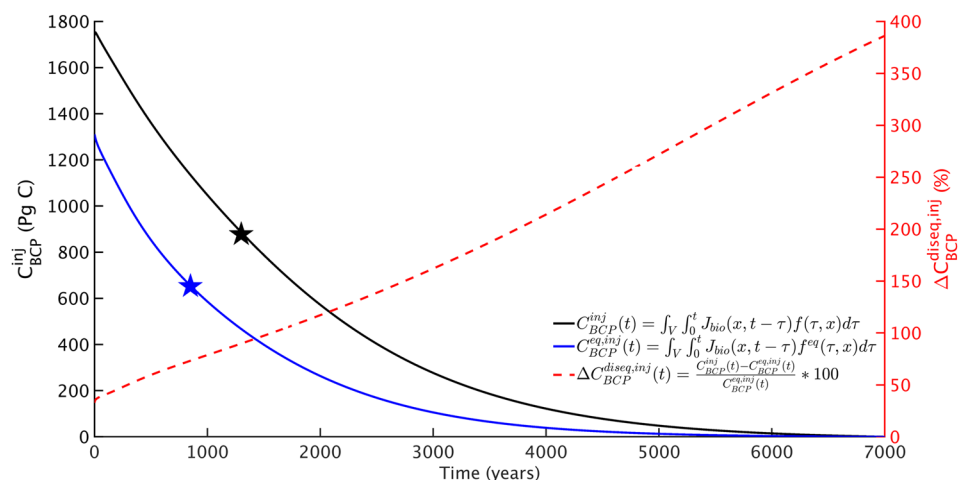


Figure 5. Global inventory of biogenic dissolved inorganic carbon (DIC) that remains sequestered for at least t years. This quantity is obtained by subtracting the globally integrated amount of carbon that is sequestered for t years or less (see Equation 11) from the total C_{BCP} . The black line represents the realistic gas exchange scenario, while the blue line represents the instantaneous gas exchange scenario. The disequilibrium effect is shown in red as the normalized percent difference between the realistic and instantaneous gas exchange scenarios. Stars indicate the amount of time after which 50% of the DIC inventory remains sequestered (blue for instantaneous and black for realistic gas exchange).

In addition to fixed depth horizons, fixed time horizons are often used to delineate “temporary” from “permanent” carbon sequestration, especially in the context of marine CO_2 removal (mCDR) strategies (e.g., NASEM, 2022). An effective time horizon of sequestration for at least 100 years has been often suggested as a reasonable target for “permanent” sequestration (IPCC, 2021; Lampitt, Achterberg, et al., 2008; NASEM, 2022). Does carbon stored by the ocean’s biological pump support this definition of permanent carbon sequestration? To examine this, we assess the amount of DIC stored by the BCP for t years or longer (Figure 5). Assuming instantaneous gas exchange, 1,190 Pg C, or about 92% of the total C_{BCP}^{eq} , is sequestered for 100 years or longer (Figure 5). With realistic gas exchange rates, our results suggest that 1,680 Pg C, or 96% of the total C_{BCP} , is sequestered for at least 100 years. This means that only about 4% of the biogenic DIC inventory, or slightly less than 100 Pg C in the case of realistic gas exchange, is stored for less than 100 years.

Furthermore, the enhancing effect of the air-sea CO_2 disequilibrium on biogenic carbon sequestration becomes more important for carbon that is sequestered on long timescales. For example, for carbon sequestered for 0 years or longer (i.e., the entire C_{BCP} inventory), the disequilibrium effect is roughly 35% (see Table 2), but for carbon sequestered for >1,000 years, air-sea CO_2 disequilibrium enhances C_{BCP} by 80% (Figure 5). The reason for the increasing importance of the air-sea CO_2 disequilibrium with increasing sequestration times is that the longer sequestration pathways are associated with deep waters that tend to upwell preferentially in the Southern Ocean (Marshall & Speer, 2012; Talley, 2013), which is a region of large air-sea CO_2 disequilibrium (Ito & Follows, 2013; Takahashi et al., 2009).

Although the carbon sequestration inventories presented here are specific to the mean state of the biological pump in the contemporary ocean (see Section 4.3 for further discussion of this caveat), the sequestration times for CO_2 injected in the water column, and the influence of air-sea CO_2 disequilibrium on the sequestration time (Figure 2) are relevant to numerous applications including many mCDR approaches (NASEM, 2022). Although an in-depth analysis of these approaches is beyond the scope of this study, in general the air-sea CO_2 disequilibrium will increase the sequestration time of injected CO_2 in the water column, making the estimates of Siegel et al. (2021), which were based on the assumption of instantaneous gas exchange, a lower-bound for direct CO_2 injection. For nutrient fertilization or other approaches that stimulate the biological pump, the impact of air-sea CO_2 disequilibrium on carbon sequestration times will depend on where the fertilization is applied, and on the depth and location of the subsequent remineralization. Fully addressing this is beyond the scope of this study, but should be a priority for future work.

4.3. Caveats

As with any modeling study, our results are subject to important caveats associated with the representation of real-world processes in a simplified computer model. One of the most significant caveats of this study is our assumption of a steady-state system. When we track the temporal evolution of the injected biogenic DIC inventory, we use a constant ocean circulation, air-sea CO₂ equilibration timescale, and biogenic DIC flux. This neglects any future (or ongoing) changes in ocean circulation, sea ice, wind speed, the Revelle buffer factor, NPP, etc., all of which would impact the inventory of biogenic carbon in the ocean. Changes in ocean circulation, such as a weakening of the Atlantic Meridional Overturning Circulation (Caesar et al., 2018), will impact τ_S^{eq} as ocean ventilation rates and pathways evolve (Holzer et al., 2020), while changes in wind speeds and the Revelle buffer factor will impact the degree of air-sea CO₂ disequilibrium and hence the disequilibrium sequestration times. For example, future ocean acidification will lead to an increase in the Revelle buffer factor (Emerson & Hedges, 2014), which, all else being equal, will lead to a reduction in the air-sea CO₂ equilibration timescale (Equation 6), and therefore a reduction in the air-sea CO₂ disequilibrium and in the disequilibrium carbon sequestration. With a Revelle factor increase of 34% by 2100, as predicted by ESMS under business-as-usual emissions (Jiang et al., 2019), we can expect a 25% decrease in the air-sea CO₂ equilibration timescale. However, the effect of these changes on carbon sequestration are not necessarily straightforward, as a higher Revelle factor in the future will lead to greater seasonality of air-sea CO₂ exchange (Hauck & Völker, 2015), a factor which we have not explored here. Another potentially important factor is future changes in the extent of sea ice coverage, which will affect ocean circulation, productivity, and the degree of air-sea disequilibrium. A reduction in sea ice coverage would expose more surface waters to the atmosphere, which could facilitate an increase in the biogenic DIC inventory due to enhanced biological productivity and carbon export (Morley et al., 2020). However, a reduction in sea ice could also result in a decrease in DIC_{BCP} due to increased outgassing of upwelled DIC, which would have otherwise been prevented by sea ice.

In addition to the lack of interannual variability in our model, the steady-state assumption also leaves any intra-annual (seasonal) variability in these processes unresolved. As discussed previously (see Section 4.1), any biases resulting from unresolved seasonality in the model would likely be greatest in high-latitude regions like the Southern Ocean, where processes such as deep-water formation and sea ice coverage (as well as biological activity) are highly seasonal. However, similar to the effects of interannual variability, the interactions of these seasonally variable processes are complex, and their overall impact on biogenic carbon sequestration remains uncertain. Resolving the effects of seasonality on the metrics presented here should be a priority for future research, especially given the importance of the Southern Ocean in enhancing the strength of the biological pump due to air-sea CO₂ disequilibrium.

Another source of uncertainty in our calculation results from the linearized CO₂ system chemistry used for the sequestration time calculations. As noted previously (see Section 3.1), there are small (~6%) discrepancies between the non-linear ocean biogeochemical and linearized anomaly model estimates of $\Delta C_{\text{BCP}}^{\text{diseq}}$. This is due to the nonlinearities in the realistic gas exchange scenario with respect to DIC, which the linearized models cannot capture, as well as the value of DIC used in the calculation of the linearized air-sea gas exchange timescale (Equation 6). Our linearization of CO₂ chemistry (see Supporting Information S1) used the observed contemporary DIC from GLODAPv2 (Lauvset et al., 2016) to compute the air-sea equilibration timescale, and these DIC values implicitly include the effects of biology and anthropogenic CO₂ accumulation on sea surface CO₂ system chemistry. If instead we use the preindustrial abiotic DIC simulated by our model, which does not include either of these effects, we find that the linearized model overestimates $\Delta C_{\text{BCP}}^{\text{diseq}}$ by about 12%. If we repeat our ocean biogeochemical model simulations using a fixed atmospheric pCO₂ of 400 μatm at equilibrium, and then use the resulting DIC_{tot} (Equation 1) to diagnose the air-sea CO₂ equilibration timescale, we find that the linearized model underestimates the effects of air-sea CO₂ disequilibrium by ~12% (401 Pg C vs. 352 Pg C). This suggests that linearized models are accurate to within about $\pm 10\%$ for estimating disequilibrium effects, depending on the DIC values used in the computation of $\tau_{\text{air-sea}}$.

Our results are also subject to the simplifications and assumptions made in the model ensemble described by Nowicki et al. (2022), which produced the biological DIC fluxes used here. In addition to the lack of seasonality in the OCIM as discussed previously that model did not resolve seasonal variability of biological fluxes, did not fully resolve flux poleward of about 65° due to data limitations, and did not represent the impact of larger metazoans such as krill and fish, which could play an important role in carbon export and sequestration (e.g., Pinti et al., 2023). The model was also based on satellite estimates of NPP, which have known deficiencies (Siegel et al., 2023). Future work will need to address the uncertainties introduced by these simplifications.

5. Conclusions

The BCP is an integral component of the ocean carbon cycle and functions as a strong natural regulator of atmospheric $p\text{CO}_2$ by transferring photosynthetically fixed organic carbon from the surface ocean to depth where it is temporarily sequestered. Due to the magnitude and importance of the BCP for global climate, we must be able to accurately quantify the inventory of carbon sequestered in the ocean due to the BCP as well as its sequestration time. Understanding this will allow us to more accurately inform climate change mitigation efforts such as marine CO_2 removal (mCDR), which is of rapidly growing interest to both scientists and policy makers (IPCC, 2021; NASEM, 2022).

Here, we extended the sequestration time approach for quantifying the biogenic DIC inventory to account for air-sea CO_2 disequilibrium. This method accurately estimates the effects of air-sea disequilibrium on biogenic DIC inventories, with $\sim 10\%$ uncertainty due to the linearization of CO_2 system chemistry. The results of these simulations suggest that the air-sea CO_2 disequilibrium increases sequestration times of biogenic DIC by potentially hundreds of years depending on the region and depth, and enhances the global inventory of biogenic DIC by $\sim 35\%$. In the Southern Ocean, air-sea disequilibrium increases the sequestration time of exported carbon by several hundred years in some locations, enhancing carbon sequestration in this region and amplifying the Southern Ocean's role in the global carbon cycle. Our results confirm previous findings that nearly half of the biogenic DIC inventory in the ocean is due to respiration above 1,000 m depth, even when accounting for air-sea CO_2 disequilibrium, which tends to reduce the biogenic DIC inventory in the upper ocean. Finally, we demonstrated that the vast majority ($>95\%$) of the biogenic DIC inventory is sequestered for more than 100 years, and that the influence of air-sea CO_2 disequilibrium becomes greater as the sequestration time increases.

A benefit of the sequestration time method used here is that it imparts additional information that cannot be obtained from traditional ocean biogeochemical models. These include the contribution of carbon export in different regions and at different depths to C_{BCP} , the mean sequestration time of exported carbon, and the sequestration time distribution of the ocean's biogenic DIC inventory for both the “equilibrium” and “disequilibrium” components of the biological pump. All of these metrics are useful not only for quantifying the strength of the ocean's natural BCP, but for considering purposeful manipulation of the biological pump for mCDR purposes. For example, our estimate of the mean sequestration time of CO_2 (e.g., Figure 2) generalizes the equilibrium sequestration times computed by Siegel et al. (2021) to account for the influence of the air-sea CO_2 disequilibrium and is useful for assessing the sequestration time of directly injected CO_2 . In addition, our maps of the sequestration time of exported carbon (e.g., Figure 3) may be useful for determining where purposeful stimulation of the biological pump can be most effective at sequestering CO_2 .

Conflict of Interest

The authors declare no conflicts of interest relevant to this study.

Data Availability Statement

All data used in this study are available in the following references. Biological DIC fluxes in Nowicki et al. (2022). Modern DIC concentration and alkalinity data from Lauvset et al. (2016). Salinity data in Antonov et al. (2010). Temperature data in Locarnini et al. (2010). Phosphate and silicate data in Garcia et al. (2010). Wind speed and sea ice cover data from the NOAA NCEP/DOE Reanalysis II model at https://psl.noaa.gov/thredds/catalog/Datasets/ncep.reanalysis/surface_gauss/catalog.html (Kanamitsu et al., 2002). The model output and plotting scripts are available in the FigShare database under accession code <https://doi.org/10.6084/m9.figshare.24826332>.

References

- Antonov, J. I., Seidov, D., Boyer, T. P., Locarnini, R. A., Mishonov, A. V., Garcia, H. E., et al. (2010). World Ocean Atlas 2009, Volume 2: Salinity. In S. Levitus (Ed.), *NOAA Atlas NESDIS* (Vol. 69, p. 184). U.S. Government Printing Office.
- Archibald, K., Siegel, D. A., & Doney, S. C. (2019). Modeling the impact of zooplankton diel vertical migration on the carbon export flux of the biological pump. *Global Biogeochemical Cycles*, 33(2), 181–199. <https://doi.org/10.1029/2018gb005983>
- Aumont, O., Maury, O., Lefort, S., & Bopp, L. (2018). Evaluating the potential impacts of the diurnal vertical migration by marine organisms on marine biogeochemistry. *Global Biogeochemical Cycles*, 32(11), 1622–1643. <https://doi.org/10.1029/2018GB005886>

Acknowledgments

M. Nowicki acknowledges support from NASA Earth and Space Science Fellowship 80NSSC18K1353. T. DeVries acknowledges support from NASA Award 80NSSC22K0155. D. A. Siegel acknowledges support from Department of Energy Award DE-AR0001559 and NASA Award 80NSSC17K0692.

- Baker, C. A., Martin, A. P., Yool, A., & Popova, E. (2022). Biological carbon pump sequestration efficiency in the North Atlantic: A leaky or a long-term sink? *Global Biogeochemical Cycles*, 36(6), e2021GB007286. <https://doi.org/10.1029/2021GB007286>
- Boyd, P. W., Claustre, H., Lévy, M., Siegel, D. A., & Weber, T. (2019). Multi-faceted particle pumps drive carbon sequestration in the ocean. *Nature*, 568(7752), 327–335. <https://doi.org/10.1038/s41586-019-1098-2>
- Caesar, L., Rahmstorf, S., Robinson, A., Feulner, G., & Saba, V. (2018). Observed fingerprint of a weakening Atlantic Overturning circulation. *Nature*, 556, 91–196. <https://doi.org/10.1038/s41586-018-0006-5>
- Carter, B. R., Feely, R. A., Lauvset, S. K., Olsen, A., DeVries, T., & Sonnerup, R. (2021). Preformed properties for marine organic matter and carbonate mineral cycling quantification. *Global Biogeochemical Cycles*, 35(1), e2020GB006623. <https://doi.org/10.1029/2020GB006623>
- Dall'Olmo, G., Dingle, J., Polimene, L., Brewin, R. J. W., & Claustre, H. (2016). Substantial energy input to the mesopelagic ecosystem from the seasonal mixed-layer pump. *Nature Geoscience*, 9(11), 820–823. <https://doi.org/10.1038/NGEO2818>
- de Lavergne, C., Madec, G., Roquet, F., Holmes, R. M., & McDougall, T. J. (2017). Abyssal ocean overturning shaped by seafloor distribution. *Nature*, 551(7679), 181–186. <https://doi.org/10.1038/nature24472>
- DeVries, T. (2014). The oceanic anthropogenic CO₂ sink: Storage, air-sea fluxes, and transports over the industrial era. *Global Biogeochemical Cycles*, 28(7), 631–647. <https://doi.org/10.1002/2013GB004739>
- DeVries, T. (2022). The ocean carbon cycle. *Annual Review of Environment and Resources*, 47(1), 317–341. <https://doi.org/10.1146/annurev-environ-120920-111307>
- DeVries, T., & Primeau, F. (2011). Dynamically and observationally constrained estimates of water-mass distributions and ages in the global ocean. *Journal of Physical Oceanography*, 41(12), 2381–2401. <https://doi.org/10.1175/JPO-D-10-05011.1>
- DeVries, T., Primeau, F., & Deutsch, C. (2012). The sequestration efficiency of the biological pump. *Geophysical Research Letters*, 39(13), L13601. <https://doi.org/10.1029/2012GL051963>
- Eggleston, S., & Galbraith, E. D. (2018). The devil's in the disequilibrium: Sensitivity of ocean carbon storage to climate state and iron fertilization in a general circulation model. *Biogeosciences*, 15(12), 3761–3777. <https://doi.org/10.5194/bg-15-3761-2018>
- Emerson, S. R., & Hedges, J. I. (2014). *Chemical oceanography and the marine carbon cycle*. Cambridge University Press.
- Ferreira, D., Marshall, J., Ito, T., & McGee, D. (2018). Linking glacial-interglacial states to multiple equilibria of climate. *Geophysical Research Letters*, 45(17), 9160–9170. <https://doi.org/10.1029/2018GL077019>
- Follows, M., & Williams, R. (2004). Mechanisms controlling the air–sea flux of CO₂ in the North Atlantic. In M. Follows & T. Oguz (Eds.), *The Ocean Carbon Cycle and Climate* (pp. 217–249). Kluwer Academic.
- Garcia, H. E., Locarnini, R. A., Boyer, T. P., Antonov, J. I., Zweng, M. M., Baranova, O. K., & Johnson, D. R. (2010). World Ocean Atlas 2009, Volume 4: Nutrients (phosphate, nitrate, silicate). In S. Levitus (Ed.), *NOAA Atlas NESDIS* (Vol. 71, p. 398). U.S. Government Printing Office.
- Guidi, L., Legendre, L., Reygondeau, G., Uitz, J., Stemmann, L., & Henson, S. A. (2015). A new look at ocean carbon remineralization for estimating deepwater sequestration. *Global Biogeochemical Cycles*, 29(7), 1044–1059. <https://doi.org/10.1002/2014GB005063>
- Hauk, J., & Völker, C. (2015). Rising atmospheric CO₂ leads to large impact of biology on Southern Ocean CO₂ uptake via changes of the Revelle factor. *Geophysical Research Letters*, 42(5), 1459–1464. <https://doi.org/10.1002/2015GL063070>
- Heuzé, C., Heywood, K. J., Stevens, D. P., & Ridley, J. K. (2013). Southern Ocean bottom water characteristics in CMIP5 models. *Geophysical Research Letters*, 40(7), 1409–1414. <https://doi.org/10.1002/grl.50287>
- Ho, D. T., Law, C. S., Smith, M. J., Schlosser, P., Harvey, M., & Hill, P. (2006). Measurements of air–sea gas exchange at high wind speeds in the Southern Ocean: Implications for global parameterizations. *Geophysical Research Letters*, 33(16), L16611. <https://doi.org/10.1029/2006GL026817>
- Holzer, M., Chamberlain, M. A., & Matear, R. J. (2020). Climate-driven changes in the ocean's ventilation pathways and time scales diagnosed from transport matrices. *Journal of Geophysical Research: Oceans*, 125(10), e2020JC016414. <https://doi.org/10.1029/2020JC016414>
- Holzer, M., DeVries, T., & de Lavergne, C. (2021). Diffusion controls the ventilation of a Pacific Shadow Zone above abyssal overturning. *Nature Communications*, 12(1), 1–13. <https://doi.org/10.1038/s41467-021-24648-x>
- IPCC. (2021). In V. Masson-Delmotte, P. Zhai, A. Pirani, S. L. Connors, C. Péan, S. Berger, et al. (Eds.), *Climate Change 2021: The Physical Science Basis. Contribution of Working Group I to the Sixth Assessment Report of the Intergovernmental Panel on Climate Change. Summary for Policymakers*. Cambridge University Press.
- Ito, T., & Follows, M. J. (2005). Preformed phosphate, soft tissue pump and atmospheric CO₂. *Journal of Marine Research*, 63(4), 813–839. <https://doi.org/10.1357/0022240054663231>
- Ito, T., & Follows, M. J. (2013). Air–sea disequilibrium of carbon dioxide enhances the biological carbon sequestration in the Southern Ocean. *Global Biogeochemical Cycles*, 27(4), 1129–1138. <https://doi.org/10.1002/2013GB004682>
- Ito, T., Follows, M. J., & Boyle, E. A. (2004). Is AOU a good measure of respiration in the oceans? *Geophysical Research Letters*, 31(17), L17305. <https://doi.org/10.1029/2004GL020900>
- Jiang, L. Q., Carter, B. R., Feely, R. A., Lauvset, S. K., & Olsen, A. (2019). Surface ocean pH and buffer capacity: Past, present, and future. *Scientific Reports*, 9(1), 18624. <https://doi.org/10.1038/s41598-019-55039-4>
- Kanamitsu, M., Kanamitsu, M., Ebisuzaki, W., Woollen, J., Yang, S.-K., Hnilo, J. J., et al. (2002). THREDDS Data Server [Dataset]. Bulletin of the American Meteorological Society. https://psl.noaa.gov/thredds/catalog/Datasets/ncep.reanalysis/surface_gauss/catalog.html
- Khatiwala, S., Schmittner, A., & Muglia, J. (2019). Air–sea disequilibrium enhances ocean carbon storage during glacial periods. *Science Advances*, 5(6), eaaw4981. <https://doi.org/10.1126/sciadv.aaw4981>
- Lampitt, R., Achterberg, E., Anderson, T., Hughes, J., Iglesias-Rodriguez, M., Kelly-Gerrey, B., et al. (2008). Ocean fertilization: A potential means of geoengineering? *Philosophical Transactions of the Royal Society A: Mathematical, Physical & Engineering Sciences*, 366(1882), 3919–3945. <https://doi.org/10.1098/rsta.2008.0139>
- Lampitt, R. S., Boorman, B., Brown, L., Lucas, M., Salter, I., Sanders, R., et al. (2008). Particle export from the euphotic zone: Estimates using a novel drifting sediment trap, ²³⁴Th and new production. *Deep-Sea Research Part, 1*(55), 1484–1502. <https://doi.org/10.1016/j.dsr.2008.07.002>
- Lauvset, S. K., Key, R. M., Olsen, A., van Heuven, S., Velo, A., Lin, X., et al. (2016). A new global interior ocean mapped climatology: The 1° × 1° GLODAP version 2. *Earth System Science Data*, 8, 325–340. <https://doi.org/10.5194/essd-8-325-2016>
- Lewis, E., & Wallace, D. (1998). *Program developed for CO₂ system calculations*. Carbon Dioxide Information Analysis Center, Oak Ridge National Laboratory, U.S. Department of Energy. <https://doi.org/10.2172/639712>
- Li, Q., England, M. H., Hogg, A. M., Rintoul, S. R., & Morrison, A. K. (2023). Abyssal ocean overturning slowdown and warming driven by Antarctic meltwater. *Nature*, 615(7954), 841–847. <https://doi.org/10.1038/s41586-023-05762-w>
- Locarnini, R. A., Mishonov, A. V., Antonov, J. I., Boyer, T. P., Garcia, H. E., Baranova, O. K., et al. (2010). World Ocean Atlas 2009, Volume 1: Temperature. In S. Levitus (Ed.), *NOAA Atlas NESDIS* (Vol. 68, p. 184). U.S. Government Printing Office.
- Marinov, I., Gnanadesikan, A., Sarmiento, J. L., Toggweiler, J. R., Follows, M., & Mignone, B. K. (2008). Impact of ocean circulation on biological carbon storage in the ocean and atmospheric pCO₂. *Global Biogeochemical Cycles*, 22(3), GB3007. <https://doi.org/10.1029/2007GB002958>

- Marshall, J., & Speer, K. (2012). Closure of the meridional overturning circulation through Southern Ocean upwelling. *Nature Geoscience*, 5(3), 171–180. <https://doi.org/10.1038/NNGEO1391>
- Morley, S. A., Barnes, D. K. A., Cárdenas, C. A., Cotté, C., Gutt, J. H., Henley, S. F., et al. (2020). Global drivers on Southern Ocean ecosystems: Changing physical environments and anthropogenic pressures in an Earth System. *Frontiers in Marine Science*, 7, 547188. <https://doi.org/10.3389/fmars.2020.547188>
- Murnane, R., Sarmiento, J., & Le Quéré, C. (1999). Spatial distribution of air-sea CO₂ fluxes and the interhemispheric transport of carbon by the oceans. *Global Biogeochemical Cycles*, 13(2), 287–305. <https://doi.org/10.1029/1998GB900009>
- National Academies of Sciences, Engineering, and Medicine. (2022). *A Research Strategy for Ocean-based Carbon Dioxide Removal and Sequestration*. The National Academies Press. <https://doi.org/10.17226/26278>
- Nowicki, M., DeVries, T., & Siegel, D. A. (2022). Quantifying the carbon export and sequestration pathways of the ocean's biological carbon pump. *Global Biogeochemical Cycles*, 36(3), e2021GB007083. <https://doi.org/10.1029/2021GB007083>
- Parekh, P., Dutkiewicz, S., Follows, M. J., & Ito, T. (2006). Atmospheric carbon dioxide in a less dusty world. *Geophysical Research Letters*, 33(3), L03610. <https://doi.org/10.1029/2005GL025098>
- Passow, U., & Carlson, C. A. (2012). The biological pump in a high CO₂ world. *Marine Ecological Progress Series*, 470, 249–271. <https://doi.org/10.3354/meps09985>
- Pinti, J., DeVries, T., Norin, T., Serra-Pompei, C., Proud, R., Siegel, D. A., et al. (2023). Model estimates of metazoans' contributions to the biological carbon pump. *Biogeosciences*, 20(5), 997–1009. <https://doi.org/10.5194/bg-20-997-2023>
- Primeau, F. (2005). Characterizing transport between the surface mixed layer and the ocean interior with a forward and adjoint global ocean transport model. *Journal of Physical Oceanography*, 35(4), 545–564. <https://doi.org/10.1175/JPO2699.1>
- Redfield, A. C. (1934). On the proportions of organic derivations in sea water and their relation to the composition of plankton. In R. J. Daniel (Ed.), *James Johnstone Memorial Volume* (pp. 177–192). Liverpool University Press.
- Resplandy, L., Lévy, M., & McGillicuddy, D. J., Jr. (2019). Effects of eddy-driven subduction on ocean biological carbon pump. *Global Biogeochemical Cycles*, 33(8), 1071–1084. <https://doi.org/10.1029/2018GB006125>
- Revelle, R., & Suess, H. E. (1957). Carbon dioxide exchange between atmosphere and ocean and the question of an increase of atmospheric CO₂ during the past decades. *Tellus*, 9(1), 18–27. <https://doi.org/10.1111/j.2153-3490.1957.tb01849.x>
- Robinson, J., Popova, E. E., Yool, A., Srokosz, M., Lampitt, R. S., & Blundell, J. R. (2014). How deep is deep enough? Ocean iron fertilization and carbon sequestration in the Southern Ocean. *Geophysical Research Letters*, 41(7), 2489–2495. <https://doi.org/10.1002/2013GL058799>
- Sarmiento, J. L., & Gruber, N. (2006). Carbon cycle. In *Ocean biogeochemical dynamics* (pp. 318–391). Princeton University Press.
- Sarmiento, J. L., & Toggweiler, J. R. (1984). A new model for the role of the oceans in determining atmospheric pCO₂. *Nature*, 308(5960), 621–624. <https://doi.org/10.1038/308621a0>
- Schlitzer, R. (2002). Carbon export fluxes in the Southern Ocean: Results from inverse modeling and comparison with satellite-based estimates. *Deep Sea Research Part II: Topical Studies in Oceanography*, 49(9–10), 1623–1644. [https://doi.org/10.1016/S0967-0645\(02\)00004-8](https://doi.org/10.1016/S0967-0645(02)00004-8)
- Siegel, D. A., DeVries, T., Cetinić, I., & Bisson, K. M. (2023). Quantifying the ocean's biological pump and its carbon cycle impacts on global scales. *Annual Review of Marine Science*, 15(1), 329–356. <https://doi.org/10.1146/annurev-marine-040722-115226>
- Siegel, D. A., DeVries, T., Doney, S. C., & Bell, T. (2021). Assessing the sequestration time scales of some ocean-based carbon dioxide reduction strategies. *Environmental Research Letters*, 16(10), 104003. <https://doi.org/10.1088/1748-9326/ac0be0>
- Takahashi, T., Sutherland, S. C., Wanninkhof, R., Sweeney, C., Feely, R. A., Chipman, D. W., et al. (2009). Climatological mean and decadal change in surface ocean pCO₂ and net sea-air CO₂ flux over the global oceans. *Deep-Sea Research Part II*, 56(8–10), 554–577. <https://doi.org/10.1016/j.dsr2.2008.12.009>
- Talley, L. D. (2013). Closure of the global overturning circulation through the Indian, Pacific, and Southern Oceans: Schematics and transports. *Oceanography*, 26(1), 80–97. <https://doi.org/10.5670/oceanog.2013.07>
- Toggweiler, J. R., Murnane, R., Carson, S., Gnanadesikan, A., & Sarmiento, J. L. (2003). Representation of the carbon cycle in box models and GCMs 2. Organic pump. *Global Biogeochemical Cycles*, 17(1), 1027. <https://doi.org/10.1029/2001GB001841>
- Toggweiler, J. R., & Samuels, B. (1995). Effect of Drake Passage on the global thermohaline circulation. *Deep-Sea Research Part I*, 42(4), 477–500. [https://doi.org/10.1016/0967-0637\(95\)00012-U](https://doi.org/10.1016/0967-0637(95)00012-U)
- Wanninkhof, R., Park, G. H., Takahashi, T., Sweeney, C., Feely, R., Nojiri, Y., et al. (2013). Global ocean carbon uptake: Magnitude, variability, and trends. *Biogeosciences*, 10(3), 1983–2000. <https://doi.org/10.5194/bg-10-1983-2013>
- Williams, R. G., & Follows, M. J. (2011). *Ocean dynamics and the carbon cycle*. Cambridge University Press.
- Wilson, J. D., Andrews, O., Katavouta, A., de Melo Voríssimo, F., Death, R. M., Adloff, M., et al. (2022). The biological carbon pump in CMIP6 models: 21st century trends and uncertainties. *Proceedings of the National Academy of Sciences*, 119(29), e2204369119. <https://doi.org/10.1073/pnas.2204369119>